

Physical, electrical and magnetic properties of Cr doped $\text{Bi}_2\text{Sr}_2\text{Ca}_1\text{Cu}_{2-x}\text{Cr}_x\text{O}_y$ (Bi-2212) superconductors prepared by laser floating zone technique

Esen Gün¹ · Berdan Özkurt^{1,2} · B. Özçelik³ · M. A. Madre⁴ · A. Sotelo⁴ · J. C. Diez⁴

Received: 16 March 2017 / Accepted: 15 May 2017 / Published online: 19 May 2017
© Springer Science+Business Media New York 2017

Abstract The structural and magnetic properties evolution of Cr-doped $\text{Bi}_2\text{Sr}_2\text{CaCu}_{2-x}\text{Cr}_x\text{O}_y$ ceramics ($x=0.0, 0.05, 0.1, \text{ and } 0.25$) have been investigated using XRD, SEM, DC resistivity and M–H measurements. X-ray diffraction studies have shown that all samples are mainly composed of Bi-2212 phase, indicating that Cr can be incorporated in its crystal structure. The microstructure of the highly Cr-doped samples showed that some impurity phases appear, decreasing the conductivity between the grains. T_c (onset) and T_c (offset) have been improved for $x=0.05$ Cr doping, while 0.25 Cr doped samples are not superconducting. This behavior can be associated to changes in the hole concentration and/or the magnetic nature of Cr. The magnetic properties indicate that low Cr-doping enhances the loop widths. Additionally, the critical current densities, J_c , of samples have been calculated by using the Bean's critical state model. It has been found that there are important improvements in J_c values between 0.2 and 0.9 T applied magnetic fields for 0.05 Cr doped samples.

1 Introduction

The Bi–Sr–Ca–Cu–O superconductors family is formed by the well-known Bi-2201, Bi-2212, and Bi-2223. Among them, the Bi-2212 phase presents several advantages, as its high thermodynamic stability and easy formation. Moreover, it can be obtained as nearly single phase without the need of adding or substituting with other elements. However, the presence of intergrain weak links and the weak flux pinning capability in bulk materials are still drawbacks for reaching high critical current density (J_c) values in these materials [1, 2]. As it is well known, the enhancement of J_c is one of the most important issues for their practical applications [3–8]. As a consequence, many attempts have been performed to increase their current carrying capability. Some of them have reached high J_c 's through solid-state techniques, such as high applied pressure [8]. On the other hand, directional solidification techniques, such as the Laser Floating Zone (LFZ) [9–13], or the electrically assisted laser floating zone (EALFZ) [14, 15] have produced high density samples with well oriented grains, dramatically raising electrical transport properties.

In particular, it has been reported that samples grown at 15 mm/h using the LFZ method provides the highest grain alignment without internal cracks [16, 17]. Moreover, these improvements can be further enhanced by using doping or wet chemistry preparation methods, which can affect the charge carrier density [18–32]. This is an important parameter, as it is well known that the superconducting properties are improved by increasing the hole concentration per Cu atom in the Cu–O planes [33]. However, when the optimal hole concentration is exceeded, it is possible to destroy superconductivity [34–38].

In this work, the effect of Cr doping on the properties of 15 mm/h LFZ grown Bi-2212 ceramics has been studied.

✉ Berdan Özkurt
berdanozkurt@mersin.edu.tr

¹ Department of Nanotechnology and Advanced Materials, Graduate School of Natural and Applied Science, Mersin University, Mersin, Turkey

² Department of Energy Systems Engineering, Faculty of Tarsus Technology, Mersin University, Mersin, Turkey

³ Department of Physics, Faculty of Sciences and Letters, Çukurova University, 01330 Adana, Turkey

⁴ ICMA (CSIC-Universidad de Zaragoza), María de Luna 3, 50018 Zaragoza, Spain

Samples have been characterized using X-ray powder diffraction (XRD), scanning electron microscopy (SEM), DC electrical resistivity and magnetic-hysteresis loop measurements.

2 Materials and methods

$\text{Bi}_2\text{Sr}_2\text{CaCu}_{2-x}\text{Cr}_x\text{O}_y$ ceramics, with $x=0.0, 0.05, 0.10,$ and $0.25,$ have been prepared through a polymer solution route from commercial $\text{Bi}(\text{CH}_3\text{COO})_3$ ($\geq 99.99\%$, Aldrich), $\text{Sr}(\text{CH}_3\text{COO})_2 \cdot 1/2\text{H}_2\text{O}$ (99%, Panreac), $\text{Ca}(\text{CH}_3\text{COO})_2 \cdot \text{H}_2\text{O}$ (98%, Alfa Aesar), $\text{Cu}(\text{CH}_3\text{COO})_2 \cdot \text{H}_2\text{O}$ (98%, Panreac), and $\text{Cr}(\text{CH}_3\text{COO}) \cdot \text{H}_2\text{O}$ (99.9%, Alfa Aesar) powders. They were weighed in the appropriate proportions, and dissolved in a mixture of glacial acetic acid and water. To the resulting clear blue solution, polyethyleneimine (PEI) (Aldrich, 50 wt% water) was added, turning to deep blue immediately. The solution was then concentrated by recovering about 70% of the initial solvent in a rotary evaporator. Total solvent evaporation is produced on a hot plate at about 150°C , producing a deep blue thermoplastic paste. Further heating at about $300\text{--}350^\circ\text{C}$ decomposes the organic material through a self-combustion, with the release of CO_2 and nitrogen oxides. The brownish powder was then thermally treated at 750 and 800°C for 12 h with an intermediate manual milling in order to decompose the alkaline-earth carbonates. The final black powders were isostatically pressed in form of cylinders (~ 3 mm diameter) at about 200 MPa. The green ceramics were subsequently grown at 15 mm/h in a LFZ system using 18 rpm relative rotation between the seed and feed. Texturing conditions were selected according to previous works [39, 40].

Due to the incongruent melting of these materials, it is necessary to perform an annealing process to produce the Bi-2212 phase. It has been performed in two steps: 60 h at 860°C to form the Bi-2212 phase, followed by 12 h at 800°C to adjust the oxygen content and, finally, quenched in air to room temperature.

Samples with $x=0.0, 0.05, 0.1$ and 0.25 will hereafter be named A, B, C and D, respectively.

Electrical resistivity and magnetic measurements were carried out using a Cryogenic Limited PPMS (from 5 to 300 K). X-ray powder diffraction analyses were performed in a Rigaku Ultima IV X-Ray Diffractometer with a constant scan rate ($2^\circ/\text{min}$) in the range $2\theta=3\text{--}60^\circ$ to identify the different phases. Lattice parameters have been automatically calculated by the PDXL software version 1.6.0.1 with the ICDD version 6.0 database. Microstructural characterization was made on polished longitudinal cross-sections of annealed samples, using a scanning electron microscope (SEM, JEOL JSM 6400) equipped with an energy dispersive spectroscopy (EDX) system.

3 Result and discussion

3.1 XRD characterization

Figure 1 shows the powder XRD patterns of all samples. As it can be observed in the figure, major phase is the high- T_C Bi-2212 in all cases. Moreover, small amounts of Bi_2CaO_4 secondary phase have been detected (peaks indicated by * in the figure). Moreover, no Cr-based phases have been detected, suggesting that Cr has been incorporated into the Bi-2212 phase crystal structure. On the other hand, an increase in the XRD peaks intensity of B samples at $2\theta=24.98^\circ, 27.7^\circ, 31.24^\circ$ and 45.04° can be observed, indicating that they possess higher crystallinity [41–43].

Lattice parameters calculated from the XRD diffraction data are displayed in Table 1. The increase of a and b unit cell parameters in the Cr-substituted samples, when compared with the undoped ones, can be due to Cr incorporation in Bi-2212 crystal structure. Other feature illustrated in Table 1 is the slight decrease of $a, b,$ and c parameters in the C samples, compared with the ones with lower and higher Cr-doping. This is an unexpected result and more work should be performed in this system in order to clearly explain the crystalline parameters evolution.

3.2 SEM analysis

SEM micrographs performed on longitudinal polished sections of all samples are given in Fig. 2. In these images, it can be observed that there is a good alignment of grains along the growth direction. However, several contrasts can be seen in these samples. EDX analysis of these contrasts has allowed the identification of three different phases. Grey contrast (major one) corresponds to the superconducting Bi-2212 phase, while white and black contrasts to Bi-2201 and CaO secondary phases. These phases agree with the XRD data, with the exception of CaO, not detected with this technique, probably due to its low amount. Moreover, the amount of this secondary phase is decreased in samples B, compared with the A ones, while it increases again for higher Cr doping.

3.3 Electrical measurements

Figure 3 shows the temperature dependence of the electrical resistivity for A, B, and C samples. Due to the fact that D samples are not superconducting, their resistivity results have not been included in the figure. These results seem to disagree with the RXD results, which showed very similar patterns for all samples. On the other hand, it is well-known that the formula of this phase can be written as $\text{Bi}_2\text{Sr}_2\text{CaCu}_2\text{O}_{8+\delta}$. This δ coefficient indicates a slight excess of oxygen in the perovskite structure. Moreover, the

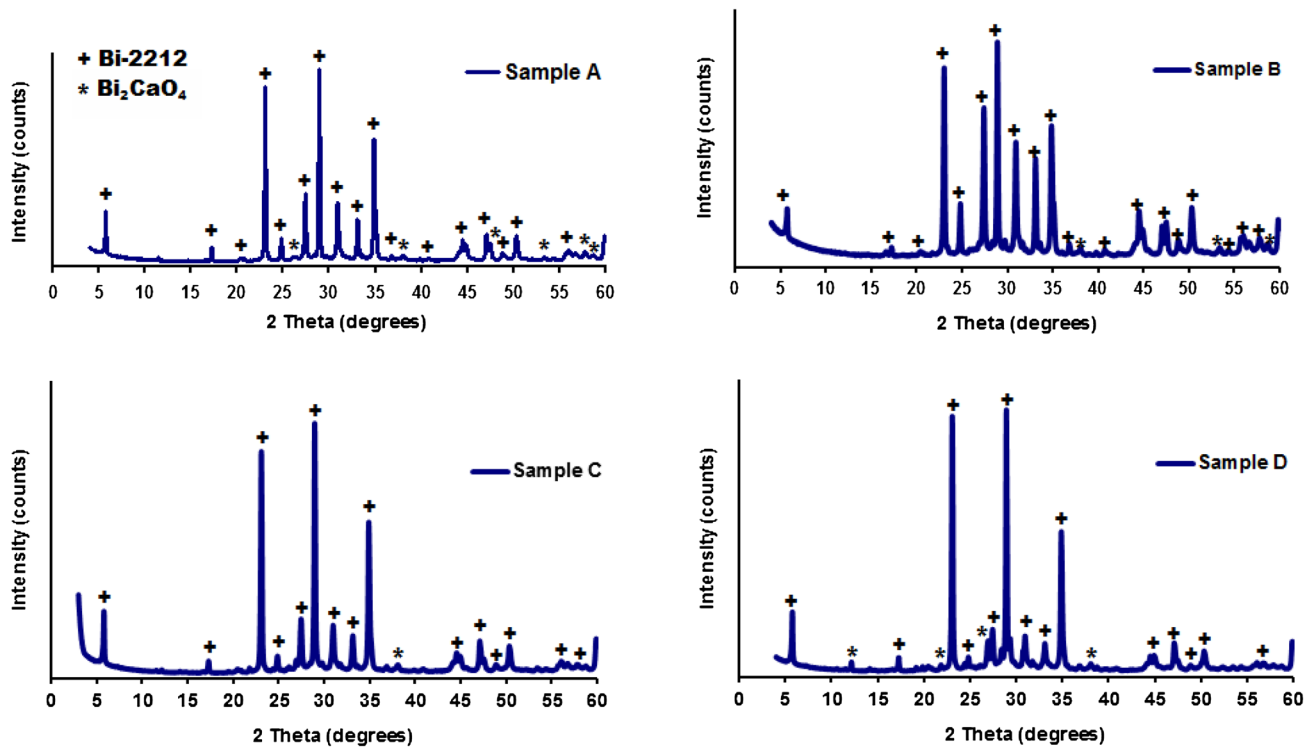


Fig. 1 Powder XRD patterns of all samples. The peaks of Bi-2212 and Bi_2CuO_4 phases are indicated by *plus* and *asterisks*, respectively

Table 1 Calculated lattice parameters for the different samples

| Samples | a (Å) | b (Å) | c (Å) |
|---------|-------|-------|--------|
| A | 3.829 | 3.829 | 30.952 |
| B | 5.413 | 5.413 | 30.854 |
| C | 5.402 | 5.402 | 30.794 |
| D | 5.417 | 5.417 | 30.877 |

superconducting properties are dramatically affected by relatively small δ value variations without modifying the crystal structure [44]. When observing the graph, T_c (onset) of all these samples is higher than 90 K, typical values for the Bi-2212 phase. However, the width of the superconducting transition (ΔT_c) for $x > 0.05$ is considerably increased (see Table 2). This effect suggests that Cr is modifying the Bi-2212 oxygen content, affecting the superconducting properties. Moreover, another effect produced by Cr addition is the modification of Bi-2212 phase melting point. These variations lead to important changes in the grain boundaries, reflected in the T_c (offset) values. It is obvious that grains connectivity is significantly decreased when Cr content is increased. On the other hand, as previously mentioned, the superconducting transition temperature depends on the charge carrier concentration. It is clear that high Cr-doping negatively affects the charge density between CuO_2 and their adjacent charge reservoir layers. From these considerations and the above data, it can be observed that

samples B are closer to the optimal charge carrier concentration than the other ones.

3.4 Magnetic properties

The magnetic-hysteresis cycles, between ± 1 T applied fields, for all the samples at 10 K, are presented in Fig. 4. M - H loops in conventional type II superconductors are extremely important in determining pinning forces as well as their diamagnetic characteristics [30, 45]. In the figure, it is evident that M_R values, as well as the M - H loops width significantly decrease when Cr content is increased. These effects clearly point out to a pinning force decrease in the Cr-doped samples. However, the path of magnetic hysteresis curves is quite similar in all Cr-doped samples, implying the formation of similar phases. Even if electrical measurements for samples D showed that they were non superconducting, they display a magnetic hysteresis loop due to the presence of Bi-2212 phase. On the other hand, a clear difference in the shape of the hysteresis loops can be observed from the undoped to the Cr-doped samples. Furthermore, in spite of these modifications, sample B seems to possess larger loop area than the undoped ones, probably due to their higher Bi-2212 phase content.

The J_C values for all samples were calculated from the hysteresis loops at 10 K, using the Bean's model [46]:

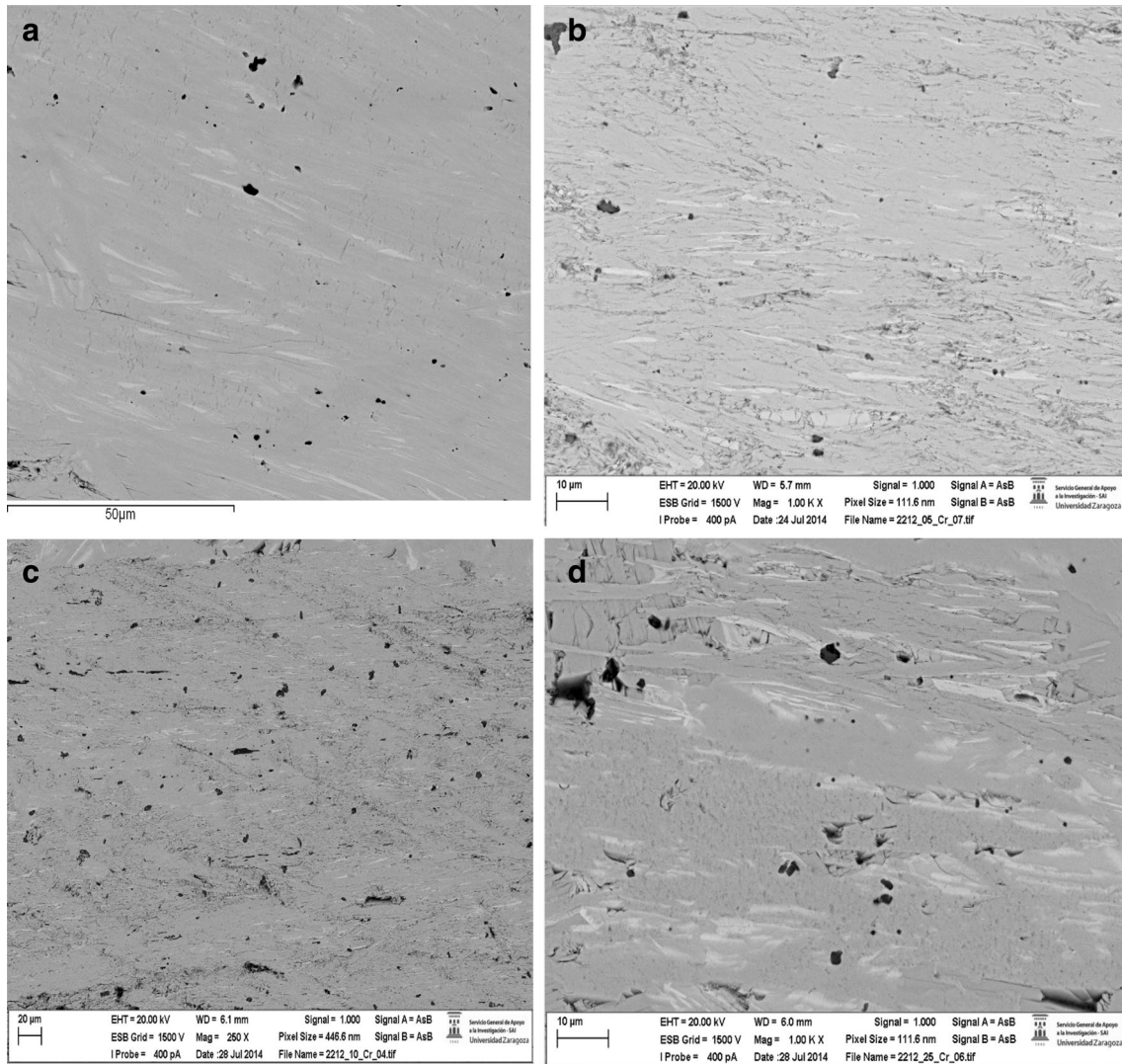


Fig. 2 SEM micrographs of polished longitudinal sections of all samples after annealing: **a** sample A; **b** sample B; **c** sample C; and **d** sample D

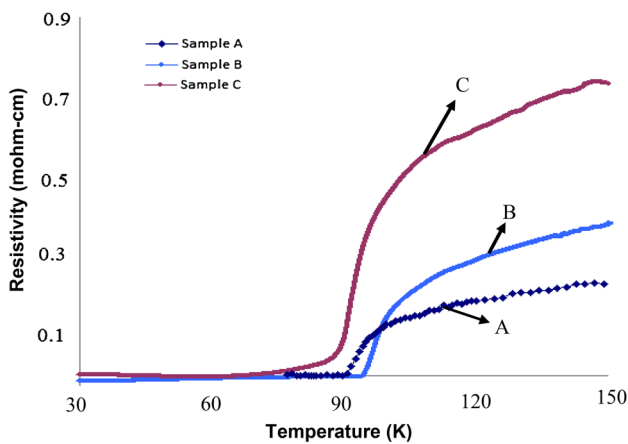


Fig. 3 Resistivity curves, as a function of temperature, for the different samples

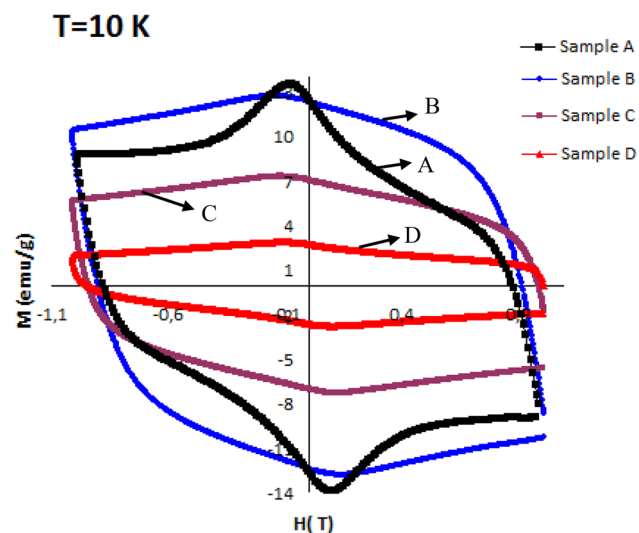
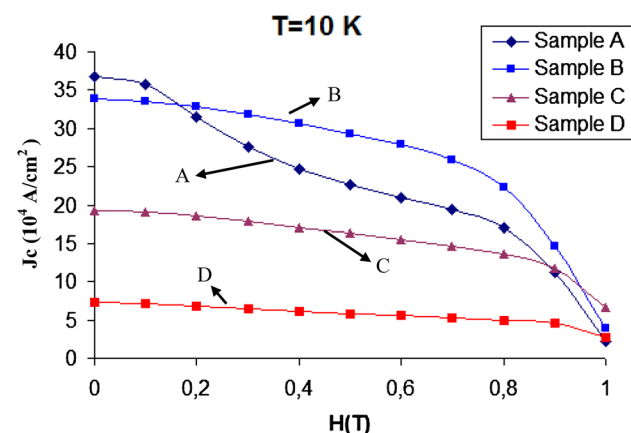
$$J_c = 30 \frac{\Delta M}{d}$$

where J_c is the magnetization current density in ampères per square centimeter. $\Delta M = M_+ - M_-$ is measured in electromagnetic units per cubic centimeter, and d is the sample thickness.

Figure 5 shows the calculated critical current densities for all samples, as a function of the applied field, at 10 K. It should be noted that resistivity results have shown that samples D are no superconducting. However, XRD results showed that samples D are majorly formed by the Bi-2212 phase, otherwise they would consist in a large halo [47]. Thus, even if calculated J_c values of these samples do not reflect a real transport critical current density, they have been represented in Fig. 5. From the figure, it is clear that samples B have the highest critical current

Table 2 Resistivity measurement results for the different samples

| Samples | T_c^{onset} (K) | T_c^{offset} (K) | ΔT_c (K) |
|---------|-------------------|--------------------|------------------|
| A | 98.8 | 92 | 6.8 |
| B | 102 | 95 | 7 |
| C | 96.8 | 71.2 | 25.6 |
| D | 91.8 | – | – |

**Fig. 4** Magnetization hysteresis curves, measured at 10 K, for all samples**Fig. 5** Calculated critical current densities for all samples at 10 K, as a function of the external applied field

values between 0.2 and 0.9 T applied magnetic fields. These results clearly indicate the formation of stronger links between the grains in samples B, compared with the A ones. This effect can be explained taking into account that weak links can be enough to maintain the continuity

of supercurrents under low magnetics. On the other hand, strong grain links are required under high magnetic fields [48, 49].

The highest J_c values (14.65×10^4 A/cm²) under 0.9 T applied magnetic field have been obtained for samples B at 10 K, suggesting that low Cr doping favours the formation of strong links between grains.

4 Conclusions

The effect of Cr doping on $\text{Bi}_2\text{Sr}_2\text{CaCu}_{2-x}\text{Cr}_x\text{O}_y$ phase ($x=0, 0.05, 0.10,$ and 0.25) has been investigated. A highest superconducting transition temperature has been found in the 0.05 Cr doped samples. Powder XRD results have revealed that all samples have similar patterns, with the Bi-2212 phase as the major one. However, the intensity of some XRD peaks for 0.05Cr-doped samples is higher than in the other ones, which can explain the observed enhancements in their T_c values. Magnetization loops ($M-H$) results have clearly shown that the width of hysteresis loops increase in 0.05 Cr doped samples. As a consequence, it can be deduced that Cr doping in low contents is useful to raise the superconducting properties of Bi-2212.

Acknowledgements This work is supported by the BAP Research Fund of Mersin University, Mersin, Turkey, under Grant Contract No: 2017-1-TP3-2176. A. Sotelo, M. A. Madre, and J. C. Diez thank Gobierno de Aragón-FEDER (Grupos de Investigacion Consolidados T12 and T87), and MINECO-FEDER (MAT2013-46505-C3-1-R) for financial support. The use of Servicio General de Apoyo a la Investigación-SAI (Universidad de Zaragoza), MEITAM Central Laboratory (Mersin University), and METU Central Laboratory (Middle East Technical University, Ankara) are also acknowledged.

References

1. Z.Y. Jia, H. Tang, Z.Q. Yang, Y.T. Xing, Y.Z. Wang, G.W. Qiao, *Physica C* **337**, 130 (2000)
2. O. Bilgili, Y. Selamet, K. Kocabaş, *J. Supercond. Nov. Magn.* **21**, 439 (2008)
3. B. Özkurt, M.A. Madre, A. Sotelo, J.C. Diez, *Physica B* **426**, 85 (2013)
4. B. Özkurt, M.A. Madre, A. Sotelo, J.C. Diez, *J. Supercond. Nov. Magn.* **26**, 3247 (2013)
5. M.E. Aytakin, B. Özkurt, İ. Sugözü, *J. Mater. Sci.* **26**, 1799 (2015)
6. B. Özcelik, B. Ozkurt, M. E. Yakinci, A. Sotelo, M. A. Madre, *J. Supercond. Nov. Magn.* **26**, 873 (2013)
7. M.E. Aytakin, B. Özkurt, K.B. Sugözü, E. Kose, İ. Sugözü, *J. Mater. Sci.* **27**, 8068 (2016)
8. D. Marconi, C. Lung, A.V. Pop, *J. Alloys Comp.* **579**, 355 (2013)
9. Y. Huang, G.F. de la Fuente, A. Sotelo, A. Badia, F. Lera, R. Navarro, C. Rillo, R. Ibanez, D. Beltran, F. Sapina, A. Beltran, *Physica C* **185**, 2401 (1991)
10. R.S. Feigelson, D. Gazit, D.K. Fork, T.H. Geballe, *Science* **240**, 1672 (1988)

11. M. Mora, A. Sotelo, H. Amaveda, M.A. Madre, J.C. Diez, F. Capel, J.M. Lopez-Cepero, J. Eur. Ceram. Soc. **27**, 3959 (2007)
12. G.F. de la Fuente, M.T. Ruiz, A. Sotelo, A. Larrea, R. Navarro, Mater. Sci. Eng. A **173**, 201 (1993)
13. V. Lennikov, B. Ozkurt, L. A. Angurel, A. Sotelo, B. Ozcelik, G. F. de la Fuente, J. Supercond. Nov. Magn. **26**, 947 (2013)
14. F.M. Costa, S. Rasekh, N.M. Ferreira, A. Sotelo, J.C. Diez, M.A. Madre, J. Supercond. Nov. Magn. **26**, 943 (2013)
15. F.M. Costa, N.M. Ferreira, S. Rasekh, A.J.S. Fernandes, M.A. Torres, M.A. Madre, J.C. Diez, A. Sotelo, Cryst. Growth Des. **15**, 2094 (2015)
16. B. Ozkurt, M. A. Madre, A. Sotelo, M. E. Yakinci, B. Ozcelik, J. Supercond. Nov. Magn. **25**, 799 (2012)
17. B. Ozkurt, M. A. Madre, A. Sotelo, M. E. Yakinci, B. Ozcelik, J. C. Diez, J. Supercond. Nov. Magn. **26**, 1093 (2013)
18. H. Sözeri, N. Ghazanfari, H. Özkan, A. Kılıç, Supercond. Sci. Technol. **20**, 522 (2007)
19. A. Sotelo, M.A. Madre, S. Rasekh, J.C. Diez, L.A. Angurel, Adv. Appl. Ceram. **108**, 285 (2009)
20. L. Jiang, Y. Sun, X. Wan, K. Wang, G. Xu, X. Chen, K. Ruan, J. Du, Physica C **300**, 61 (1998)
21. M.Z. Shoushtari, S.E.M. Ghahfarokhi, J. Supercond. Nov. Magn. **24**, 1505 (2011)
22. A.I. Abou-Aly, M.M.H. Abdel Gawad, R. Awad, I. G-Eldeen, J. Supercond. Nov. Magn. **24**, 2077 (2011)
23. B. Ozkurt, M.A. Madre, A. Sotelo, J.C. Diez, J. Mater. Sci. **24**, 3344 (2013)
24. S. Şakiroğlu, K. Kocabaş, J. Supercond. Nov. Magn. **24**, 1321 (2011)
25. S.M. Khalil, J. Phys. Chem. Solids **62**, 457 (2001)
26. A. Sotelo, M. Mora, M.A. Madre, H. Amaveda, J.C. Diez, L.A. Angurel, M.C. Mayoral, Bol. Soc. Esp. Ceram. Vidr. **45**, 228 (2006)
27. M.A. Madre, H. Amaveda, M. Mora, A. Sotelo, L.A. Angurel, J.C. Diez, Bol. Soc. Esp. Ceram. Vidr. **47**, 148 (2008)
28. Y.L. Chen, R. Stevens, J. Am. Ceram. Soc. **75**, 1150 (1992)
29. R. Ramesh, S. Green, C. Jiang, Y. Mei, M. Rudee, H. Luo, G. Thomas, Phys. Rev. B **38**, 7070 (1988)
30. B. Ozkurt, J. Alloy. Compd. **579**, 132 (2013)
31. B. Ozkurt, J. Mater. Sci. **24**, 2426 (2013)
32. F. Kahraman, A. Sotelo, M.A. Madre, J.C. Diez, B. Ozkurt, Sh. Rasekh, Ceram. Int. **41**, 14924 (2015)
33. M.R. Presland, J.L. Tallon, R.G. Buckley, R.S. Liu, N.E. Floeier, Physica C **176**, 95 (1991)
34. C. Terzioğlu, M. Yılmazlar, O. Oztürk, E. Yanmaz, Physica C **423**, 119 (2005)
35. M.A. Aksan, M.E. Yakinci, J. Alloys Compd. **433**, 22 (2007)
36. Y. Koike, Y. Iwabuchi, S. Hosoya, N. Kobayashi, T. Fukase, Physica C **159**, 105 (1989)
37. D. Yazıcı, B. Özçelik, S. Altın, M.E. Yakinci, J. Supercond. Nov. Magn. **24**, 217 (2011)
38. K. Kocabaş, S. Şakiroğlu, M. Çiftçioğlu, İ. Ercan, H. Epik, O. Bilgili, J. Supercond. Nov. Magn. **22**, 749 (2009)
39. H. Gundogmus, B. Ozcelik, A. Sotelo, M.A. Madre, J. Mater. Sci. **24**, 2568 (2013)
40. B. Özkurt, B. Özçelik, M.A. Madre, A. Sotelo, J.C. Diez, J. Mater. Sci. **26**, 5761 (2015)
41. M. Inoue, I. Hirasawa, J. Cryst. Growth **380**, 169 (2013)
42. M. Çalış, B. Özkurt, M.E. Aytekin, E. Gün, M.E. Kır, U. Öztornacı, J. Mater. Sci. **27**, 2670 (2016)
43. U. Öztornacı, B. Özkurt, Ceram. Int. **43**, 4545 (2017)
44. B. Raveau, C. Michel, M. Hervieu, D. Groult, *The Complex Chemistry of Superconductive Layered Cuprates*, In Chemistry of Superconductor Materials. T.A. Vanderah (ed.), (Noyes Publications, New Jersey, 1992), pp. 106–145
45. B.A. Albiss, I.M. Obaidat, M. Gharaibeh, H. Ghamlouche, S.M. Obeidat, Solid State Commun. **150**, 1542 (2010)
46. C.P. Bean, Phys. Rev. Lett. **8**, 250 (1962)
47. M.A. Aksan, M.E. Yakinci, J. Alloy. Compd. **385**, 33 (2004)
48. D.C. van der Laan, H.J.N. van Eck, B. ten Haken, J. Schwartz, H.H.J. ten Kate, IEEE T. Appl. Supercond. **11**, 3345 (2001)
49. D. Sharma, R. Kumar, V.P.S. Awana, Ceram. Int. **39**, 1143 (2013)